

RESEARCH ARTICLE

Determination of Sr²⁺ mobility in viscous bovine bone marrow by cryo-time-of-flight secondary ion mass spectrometry

Christine Kern  | Anna Pauli | Marcus Rohnke 

Institute of Physical Chemistry, Justus Liebig University Giessen, Giessen, Germany

Correspondence

M. Rohnke, Institute of Physical Chemistry, Justus Liebig University Giessen, Heinrich-Buff-Ring 17, 35392 Giessen, Germany.
Email: marcus.rohnke@phys.chemie.uni-giessen.de

Funding information

Deutsche Forschungsgemeinschaft, Grant/Award Number: SFB TRR 75 - M5; German Research Foundation

Rationale: In osteoporosis research, strontium ions (Sr²⁺) have emerged as promising therapeutic agent in modified bone cements for better fracture healing. Modeling of Sr²⁺ dispersion in bone could be used as a predictive tool for the evaluation of functionalized biomaterials in future. Therefore, determination of experimental parameters for Sr²⁺ transport in bone is essential. In this study, we focus on the determination of Sr²⁺ diffusion in viscous bovine bone marrow by time-of-flight secondary ion mass spectrometry (ToF-SIMS).

Methods: For this comparatively fast diffusion (FD) experiment, a specific experimental protocol of ToF-SIMS depth profiling under cryogenic conditions was developed. The validity of our experimental approach is proven by a time-dependent experimental series. Furthermore, 2D and 3D mass spectrometric imaging analysis was used to study Sr²⁺ surface and bulk distribution within bovine bone marrow.

Results: Detailed 2D and 3D mass spectrometric imaging analysis revealed that Sr²⁺ diffusion is slower in bone marrow areas with high intensity of lipid and fatty acid signals than in areas with less lipid content. The Sr²⁺ transport within this passive model can be described by Fickian diffusion. Average diffusion coefficients of Sr²⁺ in bovine bone marrow were obtained from diffusion profiles in FD areas ($D_{\text{bovine,FD}} = [2.09 \pm 2.39] \cdot 10^{-9} \text{ cm}^2 \text{ s}^{-1}$), slow diffusion areas ($D_{\text{bovine,SD}} = [1.52 \pm 1.80] \cdot 10^{-10} \text{ cm}^2 \text{ s}^{-1}$), and total area diffusion ($D_{\text{bovine,TA}} = [1.94 \pm 2.40] \cdot 10^{-9} \text{ cm}^2 \text{ s}^{-1}$).

Conclusions: We were able to show that cryo-ToF-SIMS is a useful tool for the characterization of rapid diffusion in water-containing highly viscous media. To the best of our knowledge, this is the first reported experimental approach for the investigation of the distribution of low concentrated therapeutic agents in bone marrow. Overall, our results provide important insights about Sr²⁺ diffusion in bovine bone marrow.

This is an open access article under the terms of the Creative Commons Attribution-NonCommercial License, which permits use, distribution and reproduction in any medium, provided the original work is properly cited and is not used for commercial purposes.

© 2022 The Authors. *Rapid Communications in Mass Spectrometry* published by John Wiley & Sons Ltd.

1 | INTRODUCTION

Next-generation biomaterials for bone fractures will be functionalized with drug release systems as well as antibiotic agents.¹ A promising approach is the functionalization of bone implants with bone growth-stimulating agents, such as silicon or strontium ions.^{2–11} This applies in particular in the case of osteoporosis patients, who suffer from delayed fracture healing.¹² Sr²⁺ has proven to be an effective therapeutic agent in the treatment of osteoporosis, mainly because of the double positive effect of Sr²⁺ ions on bone metabolism: They are able to inhibit osteoclastic bone resorption and simultaneously promote new bone formation by stimulating bone-building osteoblasts.^{2–7} Although orally and thus systemically administered Sr²⁺ can have serious disadvantages (e.g., undesirable side effects may occur, low bioavailability of less than 20%),^{6,13,14} biomaterials in turn are able to release Sr²⁺ locally on the fracture side after implantation. By restricting drug release to the fractured area, a lower dose is required than drug application by systemic, oral administration. Thus, side effects can be minimized. Positive effects of strontium-enriched biomaterials on bone cells^{9,15,16} and fracture healing process of osteoporotic bone, for example, induction of local activity of biomarkers relevant for bone remodeling, have been shown both *in vitro* and *in vivo*.^{3,17–19}

Development and validation of new bone implant and cement materials still require the use of animal experiments. The ethical approach to governing science that depends on animal research is the so-called 3Rs principles: replacement, reduction, and refinement.^{20–23} In short, 3Rs principles means to use no or non-sentient animals (replace), to use the absolute minimum number of animals (reduce), and to apply less harmful procedures to ensure health and well-being of research animals (refine).^{21,22} One way to replace research animals and to reduce their number in future studies is mathematical modeling of data sets rather than performing new studies.²¹ Therefore, a mathematical simulation of the release of active substances, such as strontium or silicon ions, from newly developed materials and the subsequent mobility of those substances in bone would be of significant advantage for the replacement of and reduction in animal experiments in future. To carry out such a simulation, release kinetics, which is a basic property of drug-loaded materials, must be determined beforehand.

However, online monitoring of drug release in *in vivo* experiments is methodically challenging. In fact, only two papers by Giers and McLaren et al. are published up to date.^{24,25} The authors of these studies used magnetic resonance imaging (MRI) to monitor the delivery and dispersion of a gadolinium diethylenetriamine pentaacetic acid complex from bone cement, which was placed on the outer shell of rabbit bone, into rabbit skin. The gadolinium is essential as a contrast agent for MRI, and the structure of the used ligand is similar to several antimicrobial substances like gentamicin and vancomycin.^{24,25} This method has two main disadvantages: first, the concentration of the chemical complex must be very high. It was shown that *in vivo* determination of the distribution of

molecules released locally from bone cement can be performed only shortly (a few hours) after implantation because the drug concentration drops below the detection limit because of dispersion in the environment.^{24,25} Second, a contrast agent is needed, which can falsify the drug release and dispersion behavior. In fact, only the distribution behavior of the marker can be observed with MRI and not the distribution behavior of the drug itself.²⁵

Therefore, in the case of strontium-modified biomaterials, MRI is not suitable as a method for determining Sr²⁺ dispersion in bone, which is in the focus of this work. Thus, we have to resort on *ex vivo* experiments. In previous studies, we successfully determined diffusion coefficients for Sr²⁺ in healthy and osteoporotic trabecular rat bone²⁶ as well as Sr²⁺ diffusion in healthy and osteoporotic cortical rat bone²⁷ with time-of-flight secondary ion mass spectrometry (ToF-SIMS). ToF-SIMS, a mass spectrometric imaging technique, enables the detection of organic and inorganic substances in trace concentrations with a lateral resolution of up to 50 nm in a single analysis process.²⁸ The high sensitivity and high-resolution imaging capability of ToF-SIMS have predestined this method for use in numerous studies, for example, analysis of new bone formation in a bone defect model or implant-tissue interactions.^{3,29–31}

In this study, we focus on the determination of the diffusion coefficient of Sr²⁺ in bone marrow in a passive transport model. This means that, for the sake of simplicity, we conduct our studies on biologically inactive bone marrow. First, a suitable ToF-SIMS measurement protocol must be developed and evaluated. Generally, rodents, rabbits, dogs, sheep, and monkeys are the main animals models used in osteoporosis research.^{32–36} However, for the bone marrow diffusion experiment presented here, this would have meant having to perform further animal experiments to retrieve bone marrow in sufficient quantity for the preliminary tests. As we also did not initially know whether our experimental approach would work, we decided to use easily and cheaply accessible bovine bone marrow for the development and evaluation of the method to avoid additional animal experiments, which is also in the sense of the 3Rs principle. Bone marrow generally has a large amount of lipids, independent of species.³⁷ In this context, the lipid composition and the fatty acid (FA) composition of the total lipids of the bone marrow vary depending on the animal species, tissue location, diet, and age.^{38–44} Nevertheless, in both rat and bovine bone marrow, palmitic acid, stearic acid, and oleic acid are predominant.^{37,40,42,45,46} Overall, bone marrow fat is mainly composed of triacylglycerides in all species, and phosphatidylcholine was shown to be the main phospholipid recovered in bone marrow from different species, including rats, cows, and humans.^{37,38,40,46–48} Because of these similarities in the composition of rat, cow, and human bone marrow, we found bovine bone marrow suitable to perform the first experiments of Sr²⁺ diffusion. The difficulty in our experimental approach lies in the rapid diffusion of Sr²⁺ in the aqueous and highly viscous media bone marrow.^{44,49–51} We developed a special experimental protocol for this comparatively fast diffusion (FD) experiment in which ToF-SIMS

depth profiling analyses were carried out under cryogenic conditions. Furthermore, ToF-SIMS 2D and 3D imaging analyses of bovine bone marrow were applied to study Sr^{2+} distribution on the bone marrow surface as well as within the bulk. Within a time-dependent experimental series, we determined diffusion coefficients for Sr^{2+} in different areas of bovine bone marrow, and by that the validity of our experimental approach for the investigation of diffusion in high viscous aqueous media by cryo-ToF-SIMS is proven.

2 | EXPERIMENTAL

2.1 | Preparation of bovine bone marrow

Bone marrow was collected from bovine bone slices that were purchased from a local butcher. Therefore, age, sex, and state of health of the animals were unknown. Bone marrow was removed from the bone slices using a spatula and pressed homogeneously into a sample carrier. As sample carriers, aluminum disks with drilled, blind holes (5 mm diameter, 1 mm depth, Figure 1) were used. Bone marrow surface was then smoothed with a spatula, and the sample carrier was stored in the refrigerator until measurement on the next day. Before ToF-SIMS measurements, samples were attached to the heating/cooling sample holder of a TOF-SIMS

5 (IONTOF GmbH, Münster, Germany) to enable sample cooling during measurement. To ensure optimal cold transfer, the sample carrier was attached to the sample holder via adhesive copper tape.

2.2 | Diffusion experiments with bone marrow

Diffusion experiments were conducted at room temperature. An aqueous SrCl_2 solution ($c = 1 \text{ mol/L}$, room temperature) was dropped onto bovine bone marrow surface (Figure 1A). Residence times of SrCl_2 solution on bovine bone marrow samples were 30 s, 60 s, and 120 s. Excess SrCl_2 solution was removed afterwards from the sample surface, and diffusion process was stopped by cooling samples down below -120°C inside the load lock of the ToF-SIMS instrument with liquid nitrogen. For the determination of Sr^{2+} diffusion, the diffusion time t was chosen as the addition of the residence times of SrCl_2 solution on bone marrow and the time until the sample reached a temperature of 10°C in the prechamber after removal of the SrCl_2 solution. Further details are explained in the supporting information. After reaching 0°C in the load lock of the SIMS machine, evacuation to vacuum was started and once vacuum was reached, sample was transferred to the analysis chamber of the ToF-SIMS instrument. In the main chamber, the sample was further cooled with liquid nitrogen to prevent Sr^{2+} diffusion.

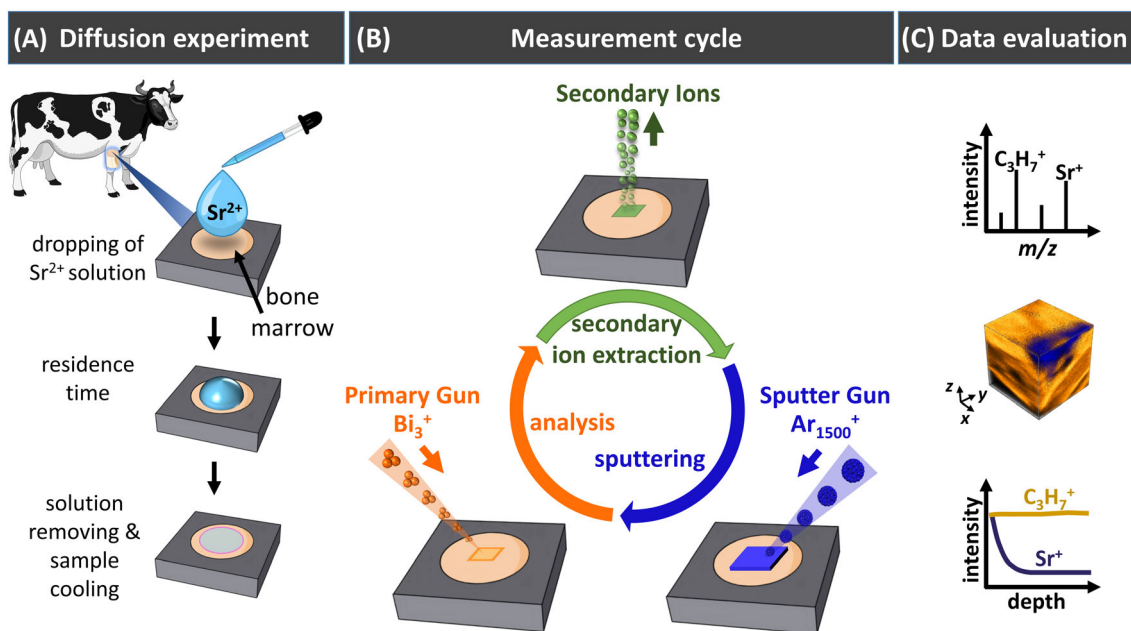


FIGURE 1 Study design of Sr^{2+} diffusion experiments with time-of-flight secondary ion mass spectrometry (ToF-SIMS). (A) Aqueous SrCl_2 solution is dropped onto bovine bone marrow surface. After specified residence times, excess strontium solution is removed, and sample is cooled down (with liquid nitrogen) to stop further Sr^{2+} diffusion into bone marrow. (B) For depth profiling, ToF-SIMS operates in the dual beam, non-interlaced mode. An analytical beam (primary ion gun) is used for analyzing a small, defined area. The secondary ions generated by the analysis beam are extracted and accelerated into the ToF analyzer. Afterwards, a high current ion beam (sputter gun) is applied for sputtering a crater which is two to three times larger than the analysis area. This measurement cycle is repeated until the diffusion profile has been completely recorded. (C) By selecting the peak of strontium (Sr^+) in the generated mass spectrum, the depth profile of Sr^+ and its 3D distribution within bone marrow are obtained. From this depth profile, diffusion coefficient D of strontium in bone marrow can be calculated [Color figure can be viewed at wileyonlinelibrary.com]

2.3 | ToF-SIMS analysis

For the determination of Sr^{2+} diffusion in bone marrow with ToF-SIMS, an IONTOF heating/cooling sample holder with the ability to reach and maintain temperatures down to -150°C was used. For all reported measurements, the sample temperature in the analysis chamber was kept below -120°C with liquid nitrogen. The measurements were performed with a ToF.SIMS 5 instrument (IONTOF GmbH, Münster, Germany) equipped with a bismuth cluster primary ion source (25 keV) and 20 keV Ar_x sputter gun. All ToF-SIMS measurements were carried out in the positive ion mode, and charge compensation was always done with a low energy electron flood gun.

2.3.1 | Depth profiling

Depth profiling of bone marrow for determining Sr^{2+} diffusion coefficients was performed in the non-interlaced mode (Figure 1B). Bi_3^+ ion clusters (25 keV) were used as primary ion species. The primary ion gun was operated in the spectrometry (high-current bunched) mode with primary ion currents between 0.2 and 0.4 pA. Scanning was performed by rastering the sample surface in a sawtooth pattern with 100 μs cycle time, 128×128 pixels, 1 shot/frame/pixel, and 1 frame/patch. The obtained mass resolution $m/\Delta m$ (FWHM) was for all measurements above 3000 at m/z C_5H_9^+ . After each analysis scan, sample surface was sputtered for 10 s with 10 keV Ar_{1500}^+ ions. Pause time for charge compensation with low energetic electrons was 5 s. Sputter beam area was $350 \times 350 \mu\text{m}^2$, with the analysis area ($100 \times 100 \mu\text{m}^2$) centered in the sputter area to avoid crater-wall-effects. The sputter current was between 8 and 13 nA. Internal mass calibration was performed using H^+ , H_2^+ , CH_3^+ , CH_4N^+ , C_2H_5^+ , C_3H_7^+ , and $\text{C}_4\text{H}_8\text{N}^+$ mass signals in positive mode.

2.3.2 | Imaging analysis

High-lateral resolution 2D (Figures 5 and 6A) as well as 3D imaging analysis (Figure 6B) were performed in the delayed extraction mode with Bi_3^+ clusters as primary ion species and delay times of 100 ns,

which was adjusted to an optimized mass signal intensity and mass resolution. Surface analysis was performed by rastering the sample surface in a sawtooth mode with the following parameters listed in Table 1. High-lateral resolution 3D imaging analysis (Figure 6B) was performed in a non-interlaced mode. Thus, after each analysis scan, the sample surface was sputtered for 10 s with 10 keV Ar_{1500}^+ cluster ions. Sputter pause was 5 s. Sputter beam area was $500 \times 500 \mu\text{m}^2$, with the analysis area centered in the sputter area to avoid crater-wall-effects. The sputter current was 9.4 nA. For mass calibration, the following signals were used for 2D and 3D imaging analyses: C_2H_5^+ , C_3H_5^+ , C_3H_7^+ , C_5H_9^+ , $\text{C}_5\text{H}_{12}\text{N}^+$, and $\text{C}_{16}\text{H}_{31}\text{O}^+$. Obtained mass resolution $m/\Delta m$ (FWHM) was for all measurements better than 3000 for the $\text{C}_7\text{H}_{13}^+$ mass signal.

2.3.3 | Data analysis

The depth of each sputter crater was measured with a confocal microscope PLu neox 3D (Sensofar, Terrassa, Spain) (exemplarily shown in Figure S1 [supporting information]). The obtained depth was used to calibrate the sputter time axis and to determine the erosion rate. We assumed a constant sputtering rate for all measurements of bovine bone marrow and for the calibration of the depth profiles. For the determination of Sr^{2+} diffusion in bovine bone marrow, four measurements were performed on bone marrow from two to three different bone pieces for each time point ($n = 4$ for 30 s, 60 s, and 120 s residence time, respectively; total number of diffusion experiments was $n = 12$).

Data analysis of the ToF-SIMS measurements was performed with Surface Lab Software version 7.2 (IONTOF GmbH, Münster, Germany).

2.4 | Statistical analysis

Mean of diffusion coefficient values from repeated tests was analyzed using Mann-Whitney U -test after ascertaining a non-normal distribution with a Shapiro-Wilk test, or one-way ANOVA after ascertaining a normal distribution. Diffusion coefficients in Table 3 are

TABLE 1 Parameters for detailed, high-resolution 2D and 3D ToF-SIMS images (Figures 5 and 6A) obtained in positive ion mode

Figure	5 (A-C)	5 (D-F)	5 (G-I)	6A	6B
Analysis options					
Cycle time (μs)	100	100	100	100	100
Field of view (μm^2)	400×400	100×100	100×100	100×100	50×50
Primary ion current (pA)	0.06	0.06	0.06	0.05	0.05
Pixels	1024×1024	512×512	512×512	512×512	256×256
Frame per patch	1	1	1	1	3
Primary ion shots/frame/pixel	1	5	2	2	10
Number of scans	100	55	180	100	50

Note. ToF-SIMS, time-of-flight secondary ion mass spectrometry.

reported as means \pm standard deviation (STD). Statistical analyses were performed using Origin v9.3 (OriginLab Corporation, Northampton, MA, USA).

3 | RESULTS

3.1 | Determination of Sr²⁺ diffusion coefficients in bovine bone marrow

Diffusion properties of Sr²⁺ ions in bovine bone marrow were analyzed using a specially developed cryo-ToF-SIMS depth profiling protocol (Figure 1). Aqueous SrCl₂ solution was dropped onto bovine bone marrow surface, and Sr²⁺ ions were allowed to diffuse into bone marrow for certain residence times (Figure 1A). Further Sr²⁺ diffusion into bone marrow was stopped by removing the strontium solution from the bone marrow surface and rapid sample cooling. Afterwards, Sr²⁺ distribution in bone marrow was characterized by ToF-SIMS depth profiling under cryogenic conditions (Figure 1B). In ToF-SIMS depth profiling, a pulsed primary ion beam produces secondary ions, which are then extracted and analyzed in a time-of-flight mass analyzer. The third step in this measurement cycle is removal of the sample surface layer by applying a sputter ion beam. The measurement cycle with alternating analyzing and sputtering steps is repeated until a complete depth profile is recorded, resulting in mass spectra, 3D mass image maps, and diffusion profiles (Figure 1C). For ensuring cryogenic conditions, the sample was maintained cool with liquid nitrogen during the whole analysis.

In SIMS analyses, strontium forms predominately positive secondary ions.⁵² Therefore, depth profiling was conducted in positive ion mode. Furthermore, in SIMS, the obtained secondary ions are primarily single charged, despite their original chemical nature. For this work, it can be further assumed that all detected strontium ion signals originate from Sr²⁺ ions (measured strontium signals are listed in Table 2). For evaluation of diffusion coefficients for Sr²⁺ diffusion in bovine bone marrow, diffusion profiles of the Sr⁺ signal were used.

To obtain a Sr²⁺ diffusion coefficient in bovine bone marrow from ToF-SIMS depth profiles, a mathematical solution of Fick's second law of diffusion (Equation [1]) was fitted to the obtained Sr⁺ signal intensities (Figure 2).

$$\frac{\partial c}{\partial t} = \frac{\partial}{\partial x} \left[D \frac{\partial c}{\partial x} \right]. \quad (1)$$

For Sr²⁺ diffusion in bovine bone marrow, we assumed diffusion from an exhaustless source into semi-infinite space as boundary conditions for solving Fick's second law of diffusion (Equation [2]), as previously described.^{26,27,53,54} Following assumptions had to be made⁵⁵:

- Because species concentration c is proportional to secondary ion intensity I in SIMS, the fit can be carried out with the obtained Sr⁺ ion signal intensities.
- The measured ion intensity I is considered as a linear function of the real Sr²⁺ intensity (I_{bg}).
- Strontium diffusion occurs from an infinite reservoir of Sr²⁺ with an intensity I_0 at the initial position x_0 .
- There are no reactions of Sr²⁺ (diffusing species) with the bone marrow matrix.

$$I(x) = I_{bg} + I_0 \times \left(1 - \operatorname{erf} \frac{x - x_0}{2\sqrt{Dt}} \right). \quad (2)$$

I_{bg} = background intensity of Sr⁺ in bone marrow

I_0 = initial intensity of the infinite source

x = position/depth

x_0 = starting point of the diffusion profile (bone marrow surface)

D = diffusion coefficient

t = diffusion time

The mass spectrometric information of each analysis layer of cryo-ToF-SIMS depth profiles was summed up as intensity versus depth diffusion profiles and afterwards plotted with the chosen mathematical fit (Equation [2]) (Figure 2). For each diffusion profile, the first data points were not considered for fitting Equation 2 to the experimental data. This is due to the fact that the first data points of ToF-SIMS depth profiles are commonly influenced by variable dopant concentrations of primary ions as well as sputter ion species. These effects result in an unsteady matrix with non-reliable secondary ion

TABLE 2 List of strontium signals identified in bovine bone marrow

Strontium signals					
m/z	Peak label	m/z	Peak label	m/z	Peak label
85.91	⁸⁶ Sr ⁺	103.90	SrO ⁺	156.87	⁸⁷ SrCl ₂ ⁺
86.91	⁸⁷ Sr ⁺	104.91	SrOH ⁺	157.87	SrCl ₂ ⁺
87.91	Sr ⁺	120.88	⁸⁶ SrCl ⁺	158.88	SrCl ₂ H ⁺
88.91	SrH ⁺	122.87	SrCl ⁺		
102.91	⁸⁷ SrO ⁺	124.87	Sr ³⁷ Cl ⁺		

Note. Analysis was performed in the positive ion mode with 25 keV Bi₃⁺ primary ion as analysis species.

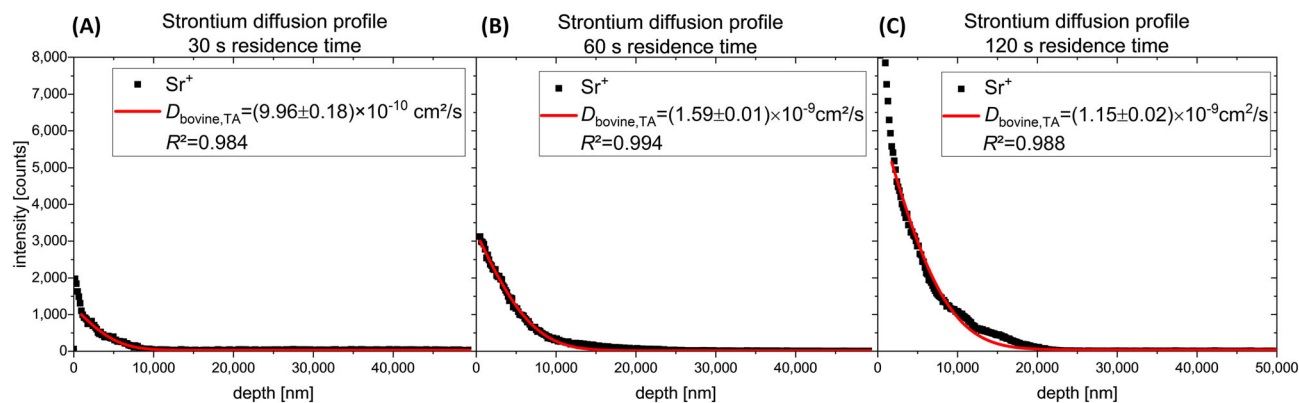


FIGURE 2 Time-of-flight secondary ion mass spectrometry (ToF-SIMS) depth profiles of Sr^{2+} diffusion in bovine bone marrow. Sr^{2+} diffusion coefficients were determined by conducting a time-dependent experimental series with strontium solution residence times on bone marrow of (A) 30 s, (B) 60 s, and (C) 120 s (exemplarily presented by one measurement for each of the time points of strontium residence). For evaluation of diffusion coefficients for Sr^{2+} diffusion in bovine bone marrow, diffusion profiles of the Sr^{+} signal were used. To obtain diffusion coefficients from total measurement area, $D_{\text{bovine,TA}}$, diffusion from an exhaustless source into semi-infinite space was assumed. The solid, red lines in (A), (B), and (C) show the results of the performed mathematical fits according to equation (2). For all depth profiles, Bi_3^{+} primary ions (25 keV) were used for analysis. Sputtering was done with a 10 keV Ar_{1500}^{+} cluster beam [Color figure can be viewed at wileyonlinelibrary.com]

TABLE 3 Time-dependent experimental series of Sr^{2+} diffusion into bovine bone marrow

Residence time	Slow diffusion $D_{\text{bovine,SD}}$	Fast diffusion $D_{\text{bovine,FD}}$	Total area diffusion $D_{\text{bovine,TA}}$	<i>n</i>
(s)	(cm^2/s)	(cm^2/s)	(cm^2/s)	
30	$(2.45 \pm 2.77) \times 10^{-10}$	$(3.72 \pm 2.83) \times 10^{-9}$	$(2.96 \pm 2.85) \times 10^{-9}$	4
60	$(1.23 \pm 0.54) \times 10^{-10}$	$(9.02 \pm 6.45) \times 10^{-10}$	$(9.39 \pm 6.80) \times 10^{-10}$	4
120	$(8.88 \pm 6.84) \times 10^{-11}$	$(1.64 \pm 2.10) \times 10^{-9}$	$(1.90 \pm 2.58) \times 10^{-9}$	4
Average value	$(1.52 \pm 1.80) \times 10^{-10}$	$(2.09 \pm 2.39) \times 10^{-9}$	$(1.94 \pm 2.40) \times 10^{-9}$	12

Note. For each residence time point, four diffusion profiles were measured with cryo-ToF-SIMS depth profiling. Diffusion coefficients (\pm STD) for different bone marrow areas (SD, slow diffusion; FD, fast diffusion; TA, total area diffusion) were determined.

data. Moreover, contamination of sample surface cannot entirely be avoided and must be considered.

Because this was the first approach of determining Sr^{2+} diffusion in bone marrow, a newly developed, time-dependent experimental series with three different residence times of Sr^{2+} solution on bovine bone marrow (30 s, Figure 2A; 60 s, Figure 2B; and 120 s, Figure 2C) was conducted to confirm a constant diffusion coefficient, which is a prerequisite for a valid diffusion experiment.

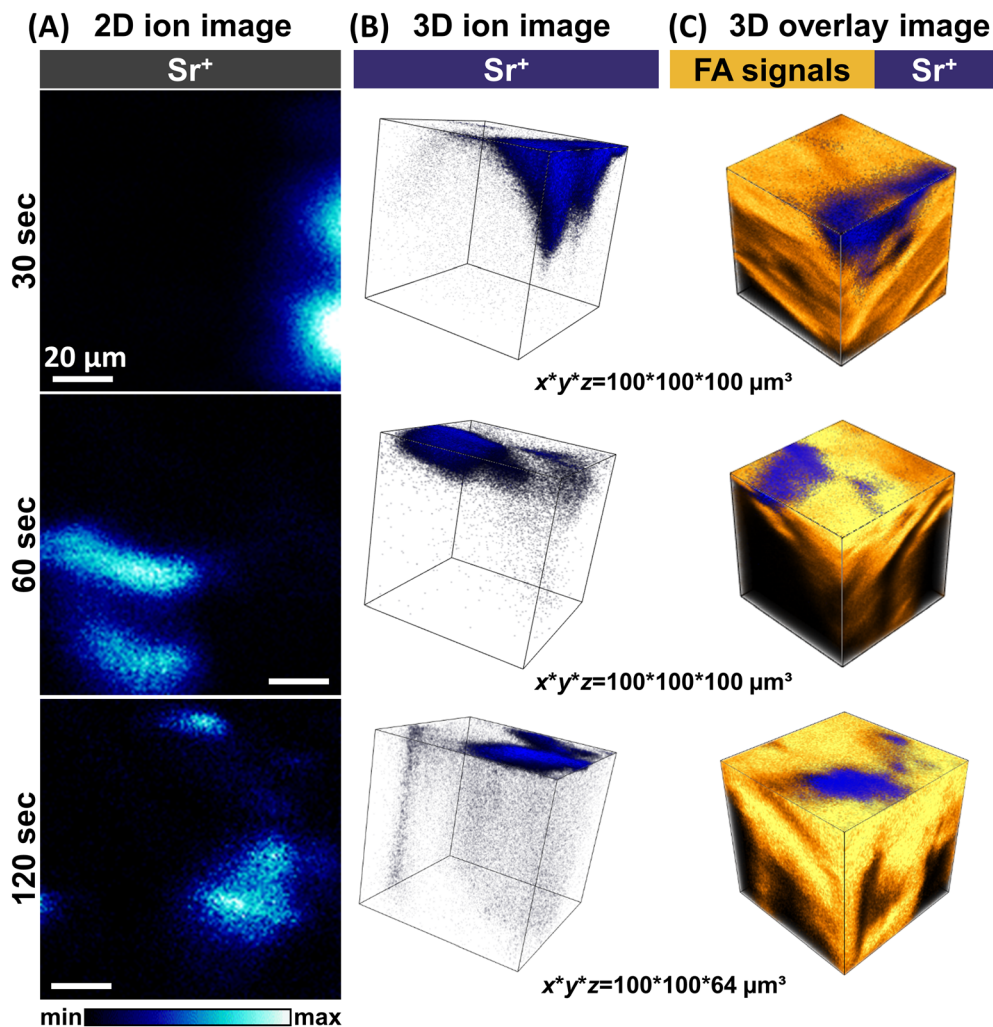
For each time point, four diffusion profiles on different bovine bone marrow samples were measured (Table 3; more detailed in Table S1 [supporting information]). The average value of Sr^{2+} diffusion coefficient in bovine bone marrow over all residence time points ($n = 12$) was $D_{\text{bovine,TA}} = (1.94 \pm 2.40) \times 10^{-9} \text{ cm}^2/\text{s}$ for total measurement area (TA). Obtained diffusion coefficients showed no time dependency within the error span (Table S1, Figure S3 [supporting information]). Therefore, we state that our experimental approach is appropriate for this study of rapid strontium diffusion in water-containing, highly viscous bone marrow.

2D (Figure 3A) and 3D ion images (Figures 3B and 3C) revealed that Sr^{2+} diffusion is not uniform throughout the total bone marrow

measurement area. For all three time points, strontium distribution was mainly found in areas with less signal intensities of FA fragments, and concentration gradients of areas of slow (low Sr^{+} intensity) and fast (high Sr^{+} intensity) diffusion were observed (Figures 3B and 3C). Lipid/FA mass signals used for Figure 3 are listed in Table S2 (supporting information).

In addition to total area diffusion, we separated those different strontium diffusion areas by applying lateral Regions of Interest (ROIs) to the ToF-SIMS imaging data. This enabled the reconstruction of diffusion profiles from areas of slow and fast strontium diffusion within bovine bone marrow (Figure 4A). For fast diffusion (FD) areas, an average diffusion coefficient of $D_{\text{bovine,FD}} = (2.09 \pm 2.39) \times 10^{-9} \text{ cm}^2/\text{s}$ was obtained (average value over all time points, $n = 12$, Figure 4B; more detailed in Figure S3 [supporting information]). For slow diffusion (SD) areas, an average diffusion coefficient of $D_{\text{bovine,SD}} = (1.52 \pm 1.80) \times 10^{-10} \text{ cm}^2/\text{s}$ was obtained (average value over all time points, $n = 12$, Figure 4B; more detailed in Figure S3 [supporting information]). The average diffusion coefficient in areas of SD was lower than the diffusion coefficient of FD areas by one order of magnitude. Statistical evaluation

FIGURE 3 2D and 3D time-of-flight secondary ion mass spectrometry (ToF-SIMS) imaging data of strontium diffusion in bovine bone marrow. (A) 2D ion images show similar diffusion behavior of Sr^{2+} for all three different time points of residence time. Sr^+ signal is mainly found in certain areas of bovine bone marrow. (B) 3D mass spectrometry data show Sr^+ intensity gradient in these areas of fast strontium diffusion. (C) 3D overlay mass images reveal that Sr^+ signal (blue) is mainly found in areas with less signal intensity of secondary ions originating from fatty acids (yellow-orange; used mass signals are found in Table S2 [supporting information]). Sputtering was done with a 10 keV Ar_{1500}^+ cluster beam; for analysis, 25 keV Bi_3^+ primary ions were used [Color figure can be viewed at wileyonlinelibrary.com]



(Mann-Whitney U -test, $*P < 0.05$) revealed a significant difference between areas of FD and SD of Sr^{2+} into bovine bone marrow (Figure 4B, $P = 0.008$). The diffusion of Sr^{2+} in total diffusion areas is mainly influenced by the FD and thus also differed significantly from SD areas (Figure 4B, $P < 0.003$; more detailed in Figure S3 [supporting information]). All diffusion coefficients are listed in Table 3 (more detailed in Table S1 [supporting information]).

3.2 | ToF-SIMS imaging of Sr^{2+} distribution in bovine bone marrow

ToF-SIMS depth profiling showed that Sr^{2+} diffuses faster into certain areas of bovine bone marrow than into others (Figure 3). By applying high-resolution ToF-SIMS imaging analysis using the delayed extraction mode, we were able to study Sr^{2+} distribution in bovine bone marrow in more detail. Because strontium forms predominately positive secondary ions,⁵² the following ToF-SIMS analyses were conducted in positive ion mode.

In bovine bone marrow, the distribution of combined strontium mass signals (Figure 5B; more detailed in F, J) is complementary to the

lateral distribution of combined signals of FA fragments (Figure 5C; more detailed G, K) and fragments originating from mono- and diacylglycerols (MAGs, DAGs) (Figure 5D; more detailed H, L). Because the intensity of MAG and DAG fragments was lower than that of FA fragments, the mass image of the sum of FA fragments was used for the overlay image (Figure 5A; more detailed E, I). Here, strontium signals are shown in blue and FA signals in yellow. In areas of high intensity of strontium secondary ions, less signal intensity of FA and lipid fragments is detected and vice versa. In comparison, combined mass signals of Na^+ and K^+ as well as cholesterol signals are in some areas co-localized with distribution of strontium signals and also not found in areas with high intensity of FA signals (Figures S4 and S6 [supporting information]). All used strontium mass signals are listed in Table 2. FA and lipid peaks used for Figure 5 are listed in Table S2 (supporting information).

High-resolution 2D secondary ion images and subsequent 3D tomography of the same ROI enable the visualization of Sr^{2+} diffusion in bovine bone marrow not only at the surface but also in depth (Figure 6). Same as in Figure 5, 2D mass images show the lateral distribution of secondary ions of the sum of strontium ion species as well as the lateral distribution of FA signals (Figure 6A). The overlay

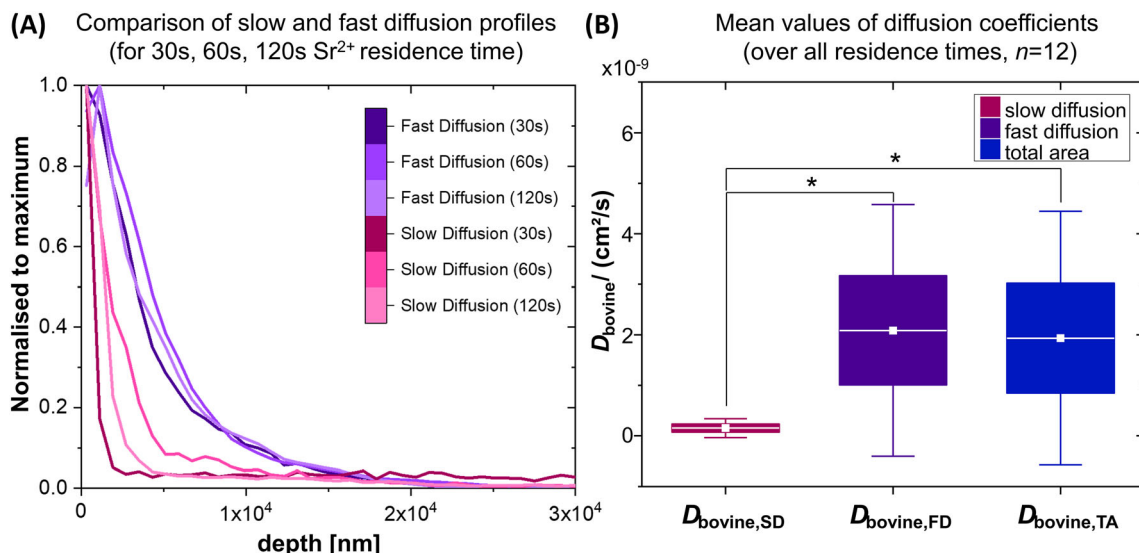


FIGURE 4 (A) Diffusion profiles from areas of slow (SD) and fast diffusion (FD) show the in-depth distribution of strontium in bovine bone marrow (exemplarily presented by one measurement for each of the time points of Sr^{2+} residence on bone marrow: 30 s, 60 s, 120 s). For comparison, strontium ion intensity was normalized to the maximum of each diffusion profile and plotted versus depth. Here, diffusion profiles of the Sr^{+} signal were used. In areas of FD, strontium ions diffused about 15 μm into bovine bone marrow. In areas of SD, strontium ions diffused between 2 and 10 μm into bovine bone marrow. (B) Comparison of the experimentally obtained diffusion coefficients of strontium diffusion in bovine bone marrow in SD areas ($D_{\text{bovine,SD}}$), FD areas ($D_{\text{bovine,FD}}$), and total diffusion areas ($D_{\text{bovine,TA}}$) ($n = 12$, respectively; detailed values are listed in Table 3 and Table S1 [supporting information]). The mean diffusion coefficient for areas of fast strontium diffusion is significantly different by one order of magnitude from the mean diffusion coefficient for areas of SD ($P < 0.008$). The diffusion in total measurement areas, mainly influenced by FD, also differs significantly from the SD ($P < 0.003$) (Mann-Whitney U -test, $*P < 0.05$) [Color figure can be viewed at wileyonlinelibrary.com]

image shows strontium signals in blue and FA signals in yellow. Again, secondary ion signals from strontium species display a surface distribution that is complementary to the distribution of FA and lipid fragments. 3D tomography of the same measurement area shows Sr^{2+} diffusion (blue) in bovine bone marrow at the surface as well as in depth. Strontium is mainly seen in areas of low FA signal intensities, implicating slower Sr^{2+} diffusion in FA and lipid rich areas. All used strontium mass signals are listed in Table 2. FA peaks are listed in Table S2 (supporting information).

4 | DISCUSSION

To the best of the authors' knowledge, there are currently no methods reported in the literature for studying ion diffusion and spatial distribution in such a highly viscous and complex medium as bone marrow. Therefore, this is the first time that the diffusion of Sr^{2+} into bone marrow has been characterized by secondary ion mass spectrometry.

Investigation of strontium diffusion in bone marrow is non-trivial, because of its quite complex cellular composition. Bone marrow generally exists in two different states.^{49–51,56} In the predominately hematopoietic osteogenic state, also called red bone marrow, it mostly contains hematopoietic cells (red/white blood cells, platelets)^{44,49,50} as well as the highly organized stroma. This stroma comprises tissue that is not directly involved in hematopoiesis, but

rather supports the proliferation of hematopoietic cells.⁴⁴ Cell types that form the bone marrow stroma include mesenchymal stem cells, fibroblasts, adipocytes, osteoblasts, osteoclasts, macrophages, or endothelial cells.⁴⁴ During bone maturation, the number of bone marrow adipocytes (BMA) increases up to approximately 70%–80% and red bone marrow converts to the second state, the so-called yellow bone marrow.^{49–51} In summary, bone marrow is a complex, lipid-rich, and water-containing tissue with high viscosity, which makes the experimental determination of the diffusion of Sr^{2+} in the bone marrow challenging. Because of the inhomogeneous composition of bone marrow, it is plausible that Sr^{2+} shows different diffusion behavior for different areas, because the different chemical composition would lead to a different interaction with the transported Sr^{2+} ions. Moreover, cell membranes could block passive Sr^{2+} transport, because those lipid bilayers are typically impermeable to larger polar molecules or ions.⁵⁷ Indeed, ToF-SIMS analyses showed different Sr^{2+} diffusion behavior for different areas of bone marrow by imaging the spatial distribution of strontium mass signals in 2D and 3D (Figures 3, 5, and 6). Lower signal intensity of strontium signals was detected in areas with high intensity of FA/lipid signals. This supports the hypothesis that cell membranes, whose bilayers are mainly composed of FAs and lipids, prevent the passive diffusion of Sr^{2+} .

For the determination of Sr^{2+} diffusion coefficients in slow, fast, and total bone marrow areas, our ToF-SIMS depth profiling protocol under cryogenic conditions, developed specifically for this

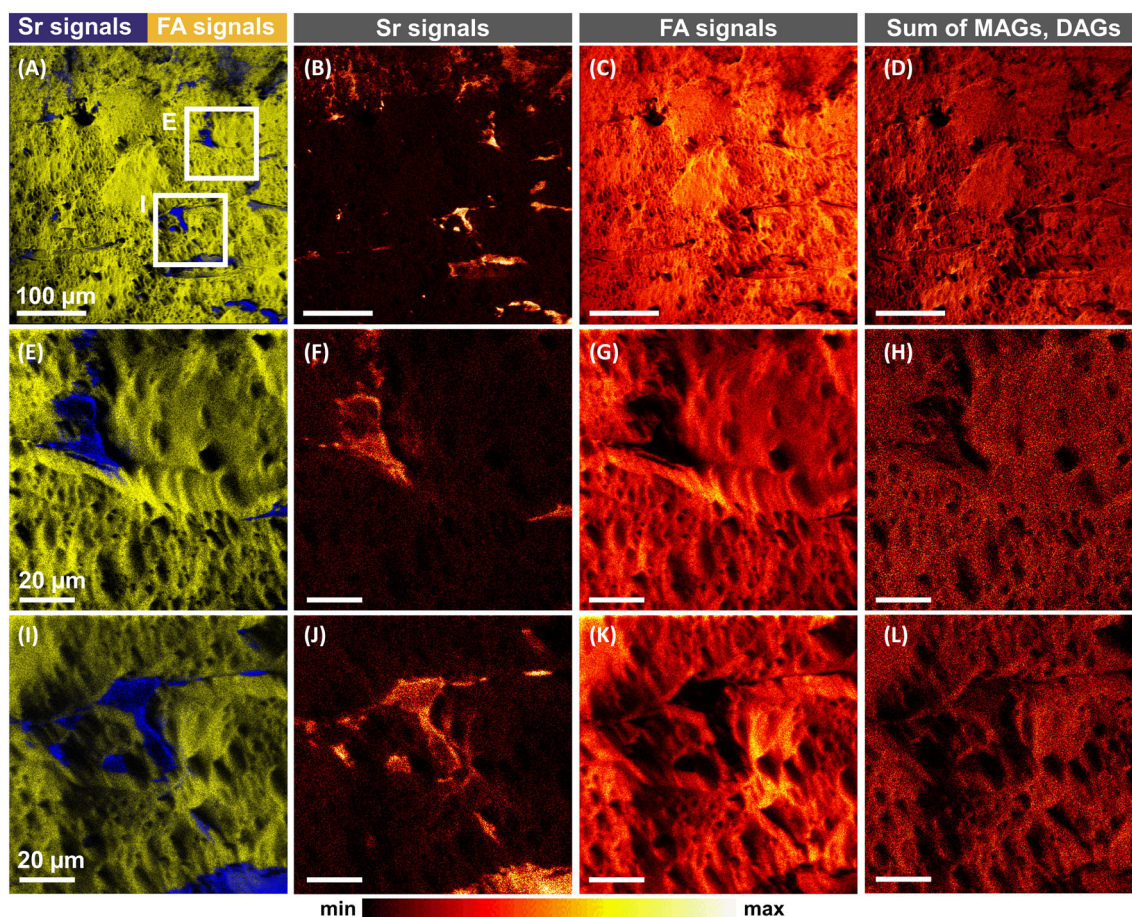


FIGURE 5 Time-of-flight secondary ion mass spectrometry (ToF-SIMS) images of strontium distribution in bovine bone marrow analyzed in the high-resolution delayed extraction mode (positive ion mode). (A) Overlay images (more detailed E, I) show distribution of strontium signals in blue and secondary ion signals from fatty acid (FA) fragments in yellow. (B) Secondary ion image shows lateral distribution of strontium mass fragments (more detailed F, J) with high intensity only in certain areas of bovine bone marrow. (C) Summed mass signals which originated from FA fragments (more detailed G, K) and (D) fragments originating from mono- and diacylglycerols (MAGs, DAGs) (more detailed H, L) show complementary distribution to strontium signals. Strontium mass signals are listed in Table 2. FA, MAG, and DAG mass signals are listed in Table S2 [supporting information]. Analyses were performed with Bi_3^+ clusters as primary ion species and a beam energy of 25 keV [Color figure can be viewed at wileyonlinelibrary.com]

comparatively fast diffusion experiment, was successfully performed on bovine bone marrow. The fact that the obtained diffusion coefficients did not vary with the residence time proves the validity of our presented method. However, the method is already close to its limit concerning the determination of diffusion coefficients in such soft media. Actually, we carried out depth profiles with depths of up to 120 μm , which needed about one working day of measurement time each. Depth profiling of bone marrow is therefore possible only within a reasonable period of time, because bone marrow is quite soft and shows a high erosion rate during sputtering. Both residence time and the cooling process are already optimized for the existing setup. If we consider these boundary conditions, we can calculate an upper diffusion coefficient via the mean squared displacement equation.

$$\sqrt{\bar{x}^2} = 2Dt \quad (3)$$

$\sqrt{\bar{x}^2}$ = mean squared displacement

D = diffusion coefficient

t = diffusion time

If the diffusion coefficient would be higher than $10^{-8} \text{ cm}^2/\text{s}$, we cannot further apply our developed experimental protocol. Then either the time of the diffusion experiment (i.e., residence time of Sr^{2+} solution on bone marrow) would have to be shortened or a longer diffusion length would have to be measured. Longer diffusion lengths could, for example, be realized by the preparation of macroscopic cross sections in combination with ToF-SIMS linescans. However, this requires a complete cryo workflow without condensation of humidity, which is not trivial.

In a previous study, we estimated the value of Sr^{2+} diffusion coefficient in bone marrow, based on experimental values for water mobility in bone marrow and the diffusion coefficient of Sr^{2+} in pure

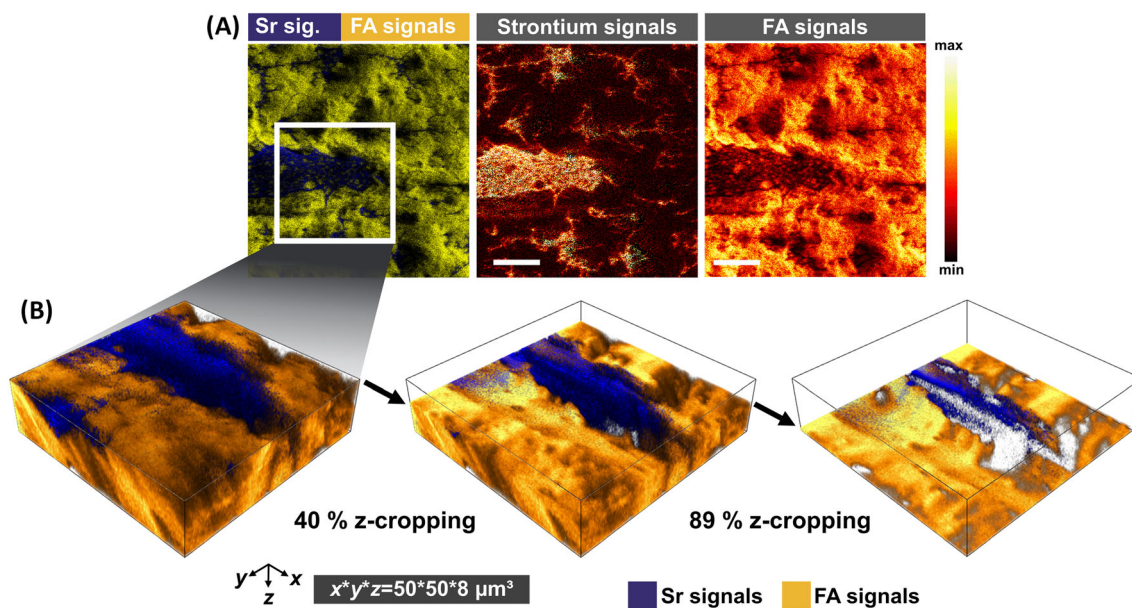


FIGURE 6 High-lateral resolution 2D imaging and 3D tomography of Sr^{2+} diffusion into bovine bone marrow. (A) 2D high-resolution secondary ion images of the sum of strontium signals and fatty acid (FA) signals. Mass overlay image shows strontium signals in blue and FA signals in yellow. Strontium signals show a surface distribution that is complementary to the distribution of secondary ions originating from FA and lipid fragments (scale bars = 100 μm). (B) 3D tomography of a smaller part of the same measurement area as in (A) shows strontium (blue) diffusion into bovine bone marrow at the surface, in the bulk at 40% z-cropping, and at 89% z-cropping. For high-resolution 2D and 3D imaging analysis, 25 keV Bi_3^+ cluster primary ions were applied in delayed extraction mode (positive ion mode) [Color figure can be viewed at wileyonlinelibrary.com]

water ($7.91 \times 10^{-6} \text{ cm}^2/\text{s}$).²⁶ When estimating the diffusion coefficient for Sr^{2+} in bone marrow in our previous study, we made the assumption that Sr^{2+} mobility in bone marrow should be lower than the mobility of the diffusion of Sr^{2+} in water as well as of water in bone marrow.²⁶ The latter was measured by diffusion-weighted MRI.^{49,58–62} The reason for this assumption is the double positive charge of the strontium ions, which should have an attractive effect on other charged ions in the bone marrow, resulting in a significantly lower, hindered mobility. Therefore, we had used a value of $1 \times 10^{-8} \text{ cm}^2/\text{s}$ for our calculations.²⁶ This value, estimated by us at that time, is only about one order of magnitude larger than the value of $(1.94 \pm 2.40) \times 10^{-9} \text{ cm}^2/\text{s}$ for Sr^{2+} diffusion in bovine bone marrow which we determined experimentally in the current ex vivo study (total area diffusion; experimentally determined diffusion coefficients are listed in Table S3 [supporting information] together with the ADC values from the literature). It should also be noted that the obtained diffusion coefficients of Sr^{2+} diffusion at room temperature are subject to error because of the experimental setup. This is due to the fact that Sr^{2+} ions continue to diffuse in the load lock of the ToF-SIMS instrument during the cooling period. The cooling phase from 21°C to 0°C lasted 50 s and the duration of cooling from 21°C to 10°C lasted 30 s. To minimize the error in the calculation of the diffusion coefficients, the time to reach a temperature of 10°C in the load lock was used to calculate the diffusion coefficients. Diffusion of Sr^{2+} decreases from 21°C to 10°C; therefore, the value of diffusion coefficients obtained is lower than the actual value of Sr^{2+} diffusion at room temperature. To minimize this discrepancy, the diffusion time

from 10°C to 0°C was not included in the calculation, although Sr^{2+} ions continue to diffuse during this period.

Overall, it has to be noted that the analytical determination of active Sr^{2+} transport via the vascular system in bone marrow in vivo is difficult to implement methodically. One way to determine the spatial distribution of a drug in vivo is by MRI. This was shown, for example, in the study by Giers et al, who observed the distribution of a marker, which was comparable in size and solubility to known antimicrobials, after its release from an implanted bone cement.²⁵ Nonetheless, a high drug concentration was a prerequisite for this, which is why the MRI studies can only be carried out a few hours after implantation, as the drug concentration drops rapidly under the detection limit due to dispersion into the environment.²⁵ Another disadvantage of this method is that only the distribution behavior of the marker could be observed and not the distribution behavior of the drug itself.²⁵ Therefore, and because in vivo drug concentration is usually very low for MRI imaging, the only way to estimate and image drug distribution with analytical methods is in post-mortem studies, as we have done here.

5 | CONCLUSION

In conclusion, within our study we could successfully establish cryo-ToF-SIMS depth profiling and high-resolution ToF-SIMS imaging analysis for the characterization of Sr^{2+} mobility in bovine bone marrow in a first approach. Despite the limitations of our study, we

were able to successfully determine the migration rate of Sr^{2+} in different areas of bovine bone marrow by passive transport in this first model of Sr^{2+} diffusion.

ACKNOWLEDGMENTS

This work was funded by the German Research Foundation (Deutsche Forschungsgemeinschaft, DFG; Collaborative Research Centre Transregio 79 – subproject M5). The authors gratefully acknowledge the financial support within this project. All authors state that they have no conflicts of interest. Open access funding enabled and organized by Projekt DEAL.

PEER REVIEW

The peer review history for this article is available at <https://publons.com/publon/10.1002/rcm.9300>.

DATA AVAILABILITY STATEMENT

SIMS data available on request from the authors.

ORCID

Christine Kern  <https://orcid.org/0000-0003-4480-4003>

Marcus Rohnke  <https://orcid.org/0000-0002-8867-950X>

REFERENCES

- Ziemia AM, Gilbert RJ. Biomaterials for local, controlled drug delivery to the injured spinal cord. *Front Pharmacol*. 2017;8:245. doi:10.3389/fphar.2017.00245
- Takahashi N, Sasaki T, Tsouderos Y, Suda T. S 12911-2 inhibits osteoclastic bone resorption in vitro. *J Bone Miner Res*. 2003;18(6):1082-1087. doi:10.1359/jbmr.2003.18.6.1082
- Thormann U, Ray S, Sommer U, et al. Bone formation induced by strontium modified calcium phosphate cement in critical-size metaphyseal fracture defects in ovariectomized rats. *Biomaterials*. 2013;34(34):8589-8598. doi:10.1016/j.biomaterials.2013.07.036
- Marie PJ, Ammann P, Boivin G, Rey C. Mechanisms of action and therapeutic potential of strontium in bone. *Calcif Tissue Int*. 2001;69(3):121-129. doi:10.1007/s002230010055
- Kokesch-Himmelreich J, Schumacher M, Rohnke M, Gelinsky M, Janek J. ToF-SIMS analysis of osteoblast-like cells and their mineralized extracellular matrix on strontium enriched bone cements. *Biointerphases*. 2013;8(1):17. doi:10.1186/1559-4106-8-17
- Li D, Chen K, Duan L, et al. Strontium Ranelate incorporated enzyme-cross-linked gelatin nanoparticle/silk fibroin aerogel for osteogenesis in OVX-induced osteoporosis. *ACS Biomater Sci Eng*. 2019;5(3):1440-1451. doi:10.1021/acsbomaterials.8b01298
- Kołodziejska B, Stępień N, Kolmas J. The influence of strontium on bone tissue metabolism and its application in osteoporosis treatment. *Int J Mol Sci*. 2021;22(12):6564. doi:10.3390/ijms22126564
- Wagner AS, Glenske K, Henß A, et al. Cell behavior of human mesenchymal stromal cells in response to silica/collagen based xerogels and calcium deficient culture conditions. *Biomed Mater*. 2017;12(4):045003. doi:10.1088/1748-605X/aa6e29
- Wagner AS, Schumacher M, Rohnke M, et al. Incorporation of silicon into strontium modified calcium phosphate bone cements promotes osteoclastogenesis of human peripheral mononuclear blood cells. *Biomed Mater*. 2019;14(2):025004. doi:10.1088/1748-605X/aaf701
- Arora M, Arora E. The promise of silicon: Bone regeneration and increased bone density. *J Arthrosc Jt Surg*. 2017;4(3):103-105. doi:10.1016/j.jajs.2017.10.003
- Fiani B, Jarrah R, Shields J, Sekhon M. Enhanced biomaterials: Systematic review of alternatives to supplement spine fusion including silicon nitride, bioactive glass, amino peptide bone graft, and tantalum. *Neurosurg Focus FOC*. 2021;50(6):E10. doi:10.3171/2021.3.FOCUS201044
- Rachner TD, Khosla S, Hofbauer LC. Osteoporosis: Now and the future. *Lancet*. 2011;377(9773):1276-1287. doi:10.1016/S0140-6736(10)62349-5
- Sips AJ, van der Vijgh WJ, Barto R, Netelenbos JC. Intestinal strontium absorption: From bioavailability to validation of a simple test representative for intestinal calcium absorption. *Clin Chem*. 1995;41(10):1446-1450. doi:10.1093/clinchem/41.10.1446
- Reginster JY. Cardiac concerns associated with strontium ranelate. *Expert Opin Drug Saf*. 2014;13(9):1209-1213. doi:10.1517/14740338.2014.939169
- Schumacher M, Henß A, Rohnke M, Gelinsky M. A novel and easy-to-prepare strontium(II) modified calcium phosphate bone cement with enhanced mechanical properties. *Acta Biomater*. 2013;9(7):7536-7544. doi:10.1016/j.actbio.2013.03.014
- Schumacher M, Wagner AS, Kokesch-Himmelreich J, et al. Strontium substitution in apatitic CaP cements effectively attenuates osteoclastic resorption but does not inhibit osteoclastogenesis. *Acta Biomater*. 2016;37:184-194. doi:10.1016/j.actbio.2016.04.016
- Alt V, Thormann U, Ray S, et al. A new metaphyseal bone defect model in osteoporotic rats to study biomaterials for the enhancement of bone healing in osteoporotic fractures. *Acta Biomater*. 2013;9(6):7035-7042. doi:10.1016/j.actbio.2013.02.002
- Kruppke B, Ray S, Alt V, et al. Gelatin-modified calcium/strontium hydrogen phosphates stimulate bone regeneration in osteoblast/osteoclast co-culture and in osteoporotic rat femur defects-in vitro to in vivo translation. *Molecules*. 2020;25(21). doi:10.3390/molecules25215103
- Zarins J, Pilmane M, Sidhoma E, Salma I, Locs J. The role of strontium enriched hydroxyapatite and Tricalcium phosphate biomaterials in osteoporotic bone regeneration. *Symmetry*. 2019;11(2):229. doi:10.3390/sym11020229
- Kirk RGW. Recovering the principles of humane experimental technique: The 3Rs and the human essence of animal research. *Sci Technol Human Values*. 2018;43(4):622-648. doi:10.1177/0162243917726579
- Sneddon LU, Halsey LG, Bury NR. Considering aspects of the 3Rs principles within experimental animal biology. *J Exp Biol*. 2017;220(Pt 17):3007-3016. doi:10.1242/jeb.147058
- Wurzel H. More than 3Rs: The importance of scientific validity for harm-benefit analysis of animal research. *Lab Anim (NY)*. 2017;46(4):164-166. doi:10.1038/labana.1220
- de Boo J, Hendriksen C. Reduction strategies in animal research: A review of scientific approaches at the intra-experimental, supra-experimental and extra-experimental levels. *Altern Lab Anim*. 2005;33(4):369-377. doi:10.1177/026119290503300404
- McLaren A, Giers MB, Fraser J, Hosack L, Caplan MR, McLemore R. Antimicrobial distribution from local delivery depends on dose: A pilot study with MRI. *Clin Orthop Relat Res*. 2014;472(11):3324-3329. doi:10.1007/s11999-014-3493-1
- Giers MB, McLaren AC, Schmidt KJ, Caplan MR, McLemore R. Distribution of molecules locally delivered from bone cement. *J Biomed Mater Res B Appl Biomater*. 2014;102(4):806-814. doi:10.1002/jbm.b.33062
- Rohnke M, Pfitzenreuter S, Mogwitz B, et al. Strontium release from Sr^{2+} -loaded bone cements and dissipation in healthy and osteoporotic rat bone. *J Control Release*. 2017;262:159-169. doi:10.1016/j.jconrel.2017.07.036
- Kern C, Quade M, Ray S, et al. Investigation of strontium transport and strontium quantification in cortical rat bone by time-of-flight

- secondary ion mass spectrometry. *J R Soc Interface*. 2019;16(151):20180638. doi:10.1098/rsif.2018.0638
28. Fletcher JS, Vickerman JC. Secondary ion mass spectrometry: Characterizing complex samples in two and three dimensions. *Anal Chem*. 2013;85(2):610-639. doi:10.1021/ac303088m
 29. Henss A, Rohnke M, el Khassawna T, et al. Applicability of ToF-SIMS for monitoring compositional changes in bone in a long-term animal model. *J R Soc Interface*. 2013;10(86):20130332. doi:10.1098/rsif.2013.0332
 30. Rohnke M, Henss A, Kokesch-Himmelreich J, et al. Mass spectrometric monitoring of Sr-enriched bone cements—From in vitro to in vivo. *Anal Bioanal Chem*. 2013;405(27):8769-8780. doi:10.1007/s00216-013-7329-8
 31. Kern C, Ray S, Gelinisky M, Bellew AT, Pirkal A, Rohnke M. New insights into ToF-SIMS imaging in osteoporotic bone research. *Biointerphases*. 2020;15(3):031005. doi:10.1116/6.0000051
 32. Egermann M, Goldhahn J, Schneider E. Animal models for fracture treatment in osteoporosis. *Osteoporos Int*. 2005;16(2):S129-S138. doi:10.1007/s00198-005-1859-7
 33. Turner AS. Animal models of osteoporosis - Necessity and limitations. *Eur Cell Mater*. 2001;1:66-81. doi:10.22203/ecm.v001a08
 34. Bonucci E, Ballanti P. Osteoporosis—Bone remodeling and animal models. *Toxicol Pathol*. 2014;42(6):957-969. doi:10.1177/0192623313512428
 35. Komori T. Animal models for osteoporosis. *Eur J Pharmacol*. 2015;759:287-294. doi:10.1016/j.ejphar.2015.03.028
 36. Syed FA, Hoey KA. Integrative physiology of the aging bone: Insights from animal and cellular models. *Ann N Y Acad Sci*. 2010;1211(1):95-106. doi:10.1111/j.1749-6632.2010.05813.x
 37. During A, Penel G, Hardouin P. Understanding the local actions of lipids in bone physiology. *Prog Lipid Res*. 2015;59:126-146. doi:10.1016/j.plipres.2015.06.002
 38. Raic A, Naolou T, Mohra A, Chatterjee C, Lee-Thedieck C. 3D models of the bone marrow in health and disease: Yesterday, today and tomorrow. *MRS Commun*. 2019;9(1):37-52. doi:10.1557/mrc.2018.203
 39. Abd-El-Aal MH, Mohamed MS. A comparative study on bone fats from different species of animals. *Food Chem*. 1989;31(2):93-103. doi:10.1016/0308-8146(89)90020-4
 40. Das SK, Scott MT, Adhikary PK. Effect of the nature and amount of dietary energy on lipid composition of rat bone marrow. *Lipids*. 1975;10(10):584-590. doi:10.1007/BF02532721
 41. Pino AM, Rodriguez JP. Is fatty acid composition of human bone marrow significant to bone health? *Bone*. 2019;118:53-61. doi:10.1016/j.bone.2017.12.014
 42. Mello FC, Field RA, Forenza S, Kunsman JE. Lipid characterization of bovine bone marrow. *J Food Sci*. 1976;41(2):226-230. doi:10.1111/j.1365-2621.1976.tb00589.x
 43. Paccou J, Penel G, Chauveau C, Cortet B, Hardouin P. Marrow adiposity and bone: Review of clinical implications. *Bone*. 2019;118:8-15. doi:10.1016/j.bone.2018.02.008
 44. Gurkan UA, Akkus O. The mechanical environment of bone marrow: A review. *Ann Biomed Eng*. 2008;36(12):1978-1991. doi:10.1007/s10439-008-9577-x
 45. Lau BY, Fajardo VA, McMeekin L, et al. Influence of high-fat diet from differential dietary sources on bone mineral density, bone strength, and bone fatty acid composition in rats. *Appl Physiol Nutr Metab*. 2010;35(5):598-606. doi:10.1139/H10-052
 46. Mulder E, De Gier J, Van Deenen LLM. Phosphatide patterns of bone marrow. *Biochim Biophys Acta*. 1962;59(2):502-504. doi:10.1016/0006-3002(62)90211-1
 47. Miller GJ, Frey MR, Kunsman JE, Field RA. Bovine bone marrow lipids. *J Food Sci*. 1982;47(2):657-660. doi:10.1111/j.1365-2621.1982.tb10144.x
 48. Wajda M. Lipid composition of human bone marrow. *Biochem J*. 1965;95(1):252-255. doi:10.1042/bj0950252
 49. Vande Berg BC, Malghem J, Lecouvet FE, Maldague B. Magnetic resonance imaging of the normal bone marrow. *Eur Radiol*. 1998;8(8):1327-1334. doi:10.1007/s003300050547
 50. Morris EV, Edwards CM. Bone marrow adipose tissue: A new player in Cancer metastasis to bone. *Front Endocrinol (Lausanne)*. 2016;7:90
 51. Karampinos DC, Ruschke S, Dieckmeyer M, et al. Quantitative MRI and spectroscopy of bone marrow. *J Magn Reson Imaging*. 2018;47(2):332-353. doi:10.1002/jmri.25769
 52. Stephan T. TOF-SIMS in cosmochemistry. *Planet Space Sci*. 2001;49(9):859-906. doi:10.1016/S0032-0633(01)00037-X
 53. Crank J, Crank EPJ. *The mathematics of diffusion*. Oxford science publications. Oxford [England]: Clarendon Press; 1979.
 54. Kern S, Kern C, Pradja MM, Düring RA, Rohnke M. Spatially resolved indiffusion behavior of Cu²⁺ and Ni²⁺ in polypropylene. *J Appl Polym Sci*. 2020;138(2):49655. doi:10.1002/app.49655
 55. Schneider C, Schichtel P, Mogwitz B, Rohnke M, Janek J. Chemical diffusion of copper in lead telluride. *Solid State Ion*. 2017;303:119-125. doi:10.1016/j.ssi.2017.02.012
 56. Zhao E, Xu H, Wang L, et al. Bone marrow and the control of immunity. *Cell Mol Immunol*. 2012;9(1):11-19. doi:10.1038/cmi.2011.47
 57. Yang NJ, Hinner MJ. Getting across the cell membrane: An overview for small molecules, peptides, and proteins. *Methods Mol Biol*. 2015;1266:29-53. doi:10.1007/978-1-4939-2272-7_3
 58. Dietrich O, Geith T, Reiser MF, Baur-Melnyk A. Diffusion imaging of the vertebral bone marrow. *NMR Biomed*. 2017;30(3). doi:10.1002/nbm.3333
 59. Liu Y, Cao L, Hillengass J, et al. Quantitative assessment of microcirculation and diffusion in the bone marrow of osteoporotic rats using VCT, DCE-MRI, DW-MRI, and histology. *Acta Radiol*. 2013;54(2):205-213. doi:10.1258/ar.2012.120508
 60. Nonomura Y, Yasumoto M, Yoshimura R, et al. Relationship between bone marrow cellularity and apparent diffusion coefficient. *J Magn Reson Imaging*. 2001;13(5):757-760. doi:10.1002/jmri.1105
 61. Hillengass J, Stieltjes B, Bäuerle T, et al. Dynamic contrast-enhanced magnetic resonance imaging (DCE-MRI) and diffusion-weighted imaging of bone marrow in healthy individuals. *Acta Radiol*. 2011;52(3):324-330. doi:10.1258/ar.2010.100366
 62. Reichenbach JR. Diffusionsbildgebung. *Rofo*. 2013;185(S 01):RK402_2. doi:10.1055/s-0033-1345985

SUPPORTING INFORMATION

Additional supporting information may be found in the online version of the article at the publisher's website.

How to cite this article: Kern C, Pauli A, Rohnke M. Determination of Sr²⁺ mobility in viscous bovine bone marrow by cryo-time-of-flight secondary ion mass spectrometry. *Rapid Commun Mass Spectrom*. 2022;36(12):e9300. doi:10.1002/rcm.9300